Research Article

iMedPub Journals
http://www.imedpub.com

Synthesis and Catalysis: Open Access
ISSN 2574-0431

2017
Vol. 2 No. 2: 9

DOI: 10.4172/2574-0431.100015

Synthesis and Characterization of Novel Zr-Al_2O_3 Nanoparticles Prepared by Microemulsion Method and Its Use as Cobalt Catalyst Support for the CO Hydrogenation Reaction

Fatima Pardo-Tarifa[1,2*], Saúl Cabrera[2], Margarita Sanchez-Dominguez[3], Robert Andersson[1] and Magali Boutonnet[1]

1 Royal Institute of Technology-KTH, School of Chemical Science and Engineering, Chemical Technology, Stockholm, Sweden
2 Universidad Mayor de San Andrés, Instituto del Gas Natural-IGN, Campus Universitario, La Paz, Bolivia
3 Centro de Investigacion en Materiales Avanzados, S.C. (CIMAV), Unidad Monterrey, Monterrey, Mexico

Corresponding author: Fatima Pardo-Tarifa

pardo@kth.se

Royal Institute of Technology-KTH, School of Chemical Science and Engineering, Chemical Technology, Teknikringen 42, SE-100 44 Stockholm, Sweden.

Tel: +46 (0)8 790 8251

Citation: Pardo-Tarifa F, Cabrera S, Sanchez-Dominguez M, et al. Synthesis and Characterization of Novel Zr-Al_2O_3 Nanoparticles Prepared by Microemulsion Method and Its Use as Cobalt Catalyst Support for the CO Hydrogenation Reaction. Synth Catal. 2017, 2:2.

Abstract

For the first time binary Zr-Al oxide nanoparticles were synthesized by co-precipitation in water-in-oil microemulsion. For comparison, a similar material was prepared by Zr impregnation on commercial alumina. After calcination, these materials and unpromoted alumina were used as cobalt catalyst supports to study and compare their structural characteristics and catalytic behavior in CO hydrogenation reaction. The supports and final cobalt catalysts were characterized by X-ray diffraction (XRD), N_2 physisorption, scanning and transmission electron microscopy (SEM and TEM), temperature programmed reduction (TPR) and H_2 chemisorption. The material synthesized by microemulsion (Zr-Al_2O_3 (ME)) presented homogeneous nanoparticles with highly dispersed zirconium, textural porosity with narrow pore size distribution and high surface area. On the other hand, the material prepared by Zr impregnation on Al_2O_3 (Zr-Al_2O_3 (IM)) produced a nonhomogeneous material with low Zr distribution and structural porosity. The cobalt deposition on these supports seems to be affected by the presence of zirconium. In the presence of highly dispersed Zr on alumina, the cobalt interaction with the support is higher. On the other hand, the presence of ZrO_2 islands on alumina avoids the cobalt-support interaction favoring the cobalt reduction degree, which makes a more active catalyst in the tested reaction. The final catalysts were tested in CO hydrogenation, and a higher CO conversion was obtained with increased Co° availability on the catalyst surface. Furthermore, the selectivity was affected by the CO conversion and the physico-chemical properties of the catalyst. This study gives highlights on the synthesis of highly uniform bimetallic nanoparticles used as support for cobalt catalysts and their application.

Keywords: Zr-promoter; Zr-Al_2O_3; Water-in-oil; Microemulsion method; Cobalt catalyst; Co_3O_4 reducibility; CO hydrogenation

Received: March 05, 2017; **Accepted:** May 31, 2017; **Published:** June 15, 2017

Introduction

In the search for highly active and selective catalysts for the CO hydrogenation reaction, all elements in metallic form from group VIII are able to chemisorb and dissociate CO and H_2. However, only Ru, Co, Fe, and Ni are considered for use in commercial applications [1]. Fischer-Tropsch synthesis (FTS) is an exothermic reaction between H_2 and CO producing water and a wide variety of hydrocarbons in gas, liquid, and solid state used as fuels and chemicals [2,3]. Supported cobalt based catalysts have been used for FTS due to their higher activity, high selectivity to linear hydrocarbons, and low activity for water-gas shift (WGS) reaction [4,5]. The activity and selectivity of cobalt catalysts are dependent on metal dispersion and reduction degree, support and promoter. The interaction of cobalt and alumina is high and promoters have been incorporated in order to avoid metal-support interactions [6,7].

Zirconium seems to increase the performance of Co/Al_2O_3 catalysts [7-14]. Some authors attribute its promotion effect

to the increase of active intermediates (-CH_2-) which causes an enhancement of the catalyst activity and the selectivity to long-chain hydrocarbons [15]. Other authors found that Zr enhances the cobalt reducibility and consequently the catalyst activity [13,16,17]. On the other hand, as important as the choice of the promoter is the choice of the synthesis method. Considering the relevance of the synthesis procedure for obtaining promoted alumina supports, the microemulsion preparation method is a promising strategy. It allows the synthesis of highly homogeneous materials with controlled structural properties and particle sizes [18]. This methodology has been employed for preparation of metal nanoparticles, metal oxides and mixed metal oxides for catalytic and electrochemical processes [19,20]. The synthesis of inorganic nanoparticles in water-in-oil microemulsions is driven by microscopic micelles that act as nanoreactors where the nanoparticle synthesis occurs. A water-in-oil (W/O) microemulsion is a transparent or translucent solution which is optically isotropic and thermodynamically stable. It is made up of droplets of water surrounded by a continuous oil phase, where the interfacial tension between oil and water is overcome by the use of surfactants [18,21].

The synthesis of a variety of binary metal oxides has been studied as catalysts supports for several catalytic reactions and has shown good results due to a high homogeneity and intimate binary metal interaction. In addition, small size particles maximize the surface area exposed to the reactant, allowing more reactions to occur [22,23]

Based on the presented literature, the presence of Zr in alumina increases the CO hydrogenation reaction; however, the method of Zr incorporation intoAl_2O_3 has not been fully investigated. In addition, binary oxide nanoparticles used as supports have given good results in different application [24]. To the best of our knowledge, no Zr-Al nanoparticles co-precipitated by microemulsion method have previously been prepared and studied. Therefore the synthesis of Zr-Al oxide nanoparticles is an adequate candidate for preparing cobalt catalyst supports. The aim of this work is to synthesized as well as to study the characteristics of co-precipitated Zr-Al nanoparticles. At the same time understand how affect this material compared with similar ones on the cobalt deposition and further application as catalyst for CO hydrogenation reaction.

Experimental

Catalyst preparation

The co-precipitation of Zr-Al nanoparticles was accomplished by mixing two water-in-oil microemulsion solutions (microemulsion 1 (ME1) and microemulsion 2 (ME2)), for composition **(Table 1)**. ME1 contained Zr and Al precursors while ME2 contained the precipitating agent NH_4OH. ME2 was added to ME1 dropwise under continuous stirring at 30°C until pH 9 was reached. The solution was kept at constant conditions for 12 h to complete the reaction. The final solution was destabilized with acetone and the solid product was separated by centrifugation and washed with acetone and water. The product was freeze-dried in order to avoid the particles agglomeration. Afterwards, the product was calcined in air for 6 h at 550°C (heating rate 10°C/min). The obtained material was labeled as Zr-Al_2O_3 (ME).

Table 1 Selected composition of the microemulsion systems.

ME	Phase	Compound(s)	Composition (wt %)
ME1	Oil	Hexane	65.7
	Surfactant	Brij©	26.4
	Aqueous Solution	1M ($AlCl_3 \cdot 6H_2O$-$ZrO(NO_3)_2$) molar ratio of Zr:Al = 1:8)	7.9
ME2	Oil	Hexane	65.7
	Surfactant	Brij©	26.4
	Aqueous solution	NH_4OH 38 wt%	7.9

For comparison, Al_2O_3 and Zr/Al_2O_3 were also prepared. A commercial pseudo-boehmite Al_2O_3 (Versal 250) was dried at 120°C for 5 h and calcined at 550°C for 6 h. Afterwards, an aqueous solution of $ZrO(NO_3)_2$ was prepared and added to the treated alumina by incipient wetness impregnation (molar ratio Al:Zr=8). The material was thermally treated in the same way as Zr-Al_2O_3(ME). The obtained material was labeled as Zr-Al_2O_3(IM).

The carriers (Zr-Al_2O_3 (ME), Zr-Al_2O_3(IM) and Al_2O_3) were dried at 120°C for 5 h prior to the 12 wt% of cobalt deposition. An aqueous solution of $Co(NO_3)_2 \cdot 6H_2O$ with volume equivalent to the pore volume of each support was added to the supports dropwise. The carrier pore volume was determined by N_2-adsorption technique. After metal impregnation, the materials were dried for 6 h at 120°C and calcined in air at 350°C for 10 h (heating rate: 1°C/min). The final catalysts were labeled as Co/Zr-Al_2O_3(ME), Co/Zr-Al_2O_3(IM) and Co/Al_2O_3.

Catalyst characterization

X-ray diffraction (XRD) of the fresh samples was performed on a Siemens D5000 X-ray diffractometer with Cu Kα radiation (40 kV, 30 mA). The measurements were recorded from 10° to 90° in the 2θ range using a step size of 0.020° and a step time of 12s for all the samples. The phases were identified by the Eva software (version 13.0.0.2, 2007). Crystallite sizes of Co_3O_4 were calculated using the Scherrer equation and assuming spherical particles [25]. The Co° crystallite size was estimated from Co_3O_4 using the formula $d(Co°)=0.75 \cdot d(Co_3O_4)$ [26,27]. The analyses were performed in a pressure interval between 20 and 510 mm Hg. Chemisorption isotherms were extrapolated at zero pressure in order to determine the adsorption of hydrogen [28]. The stoichiometry assumption was that two cobalt atom per molecule of hydrogen. The average particle size of Co°, was estimated according to d(Co°)H=96 D · DOR, assuming spherical shape [29,30].

Brunauer–Emmet–Teller (BET) surface area and porosity data was collected with a Micromeritics ASAP 2000/2020 unit. 0.2 g of the samples was outgassed at 250°C overnight prior to analysis. The data was recorded by N_2 adsorption at liquid nitrogen temperature at relative pressures between 0.06 and 0.2.

The reducibility of the catalysts was investigated by hydrogen temperature-programmed reduction (H_2-TPR) [31]. The calcined catalysts (0.15 g) were studied in a Micromeritics Autochem

2910 at a flow of 5 vol% H_2 in Ar in a range of temperatures from 30°C to 930°C (heating rate: 10°C/min). The H_2 consumption was monitored during the study by the difference in thermal conductivity between the inlet and outlet gases. The degree of reduction (DOR, %) was calculated using H_2-TPR of the *in-situ* reduced catalysts. 0.15 g of the fresh catalyst was reduced at 350°C (1°C/min) for 16 h in flowing H_2, then flushed with helium gas for 30 min. Afterwards, the helium was changed to 5 vol % H_2 in Ar and the temperature was increased from 350 to 930°C (10°C/min) and the H_2 consumption was monitored. The TCD was calibrated with Ag_2O as standard. The DOR was calculated assuming that unreduced cobalt after the reduction pre-treatment was in the form of Co^{2+} according to:

$$DOR = 1 - \frac{ATCD \times f}{XCo \div AWCo}$$

where A_{TCD} is the integration of the TCD signal, normalized per mass catalyst; AW_{Co} is the atomic weight of Co (58.9 g/mol), f is a calibration factor correlating the area of the TCD signal and the H_2 consumed; X_{Co} is the cobalt loading (12% Co).

The cobalt dispersion (D, %) and the cobalt crystallite size (*d*(Co°), nm), was calculated by hydrogen static chemisorption on the reduced catalysts. The measurements were performed on a Micromeritics ASAP 202°C unit at 35°C, after reducing about 0.15 g of the fresh catalysts under the same conditions as in TPR analysis (H_2 flow at 350°C for 16 h (heating rate: 1°C/min)).

The morphology of the supports and final catalysts was studied by high resolution-scanning electron microscopy (HR-SEM) using an XHR-SEM Magellan 400 instrument supplied by the FEI Company. The samples were investigated using a low accelerating voltage and no conductive coating.

Transmission electron microscopy (TEM) analysis was performed using a Philips CM300UT-FEG electron microscope with a point resolution of 0.17 nm, information limit of 0.1 nm, which was operated at 200 kV, in which images were acquired with a TVIPS CCD camera. The samples were prepared by immersing a Quantifoil R copper micro grid in a fresh catalyst dispersed in ethanol.

Catalytic testing

CO hydrogenation was tested at operating conditions similar to Fischer-Tropsch synthesis. Experiments were performed in a stainless-steel fixed-bed reactor (i.d. 9 mm) at process conditions: 210°C, 20 bar, molar H_2/CO ratio=2.1. A mixture of 1g of catalyst with a pellet size between 53–90 µm was diluted and mixed with 5 g of SiC (for an even temperature profile) and thereafter placed in the reactor [28,32]. Prior to the reaction the catalyst was activated by reducing it *in situ* with hydrogen at 350°C for 16 h at atmospheric pressure. After activation, the reactor was cooled down to 180°C and then flushed with He before increasing the pressure to 20 bar. The catalysts were tested during two periods, first at a syngas flow of 100 cm^3/min (NTP) and in the second period the gas flow was adjusted in order to obtain a CO conversion of 30% [7,32-34]. The heavy hydrocarbons and most of the water were condensed in two traps kept at 120°C and room-temperature, respectively. The product gases leaving the traps were depressurized and analyzed on-line with a gas chromatograph (GC) Agilent 6890 equipped with a thermal conductivity detector (TCD) and a flame ionization detector (FID). H_2, N_2, CO, CH_4, and CO_2 were separated by a Carbosieve II packed column and analyzed on the TCD. The percentage of CO conversion was calculated by:

$$COconv(mol\%) = \frac{CO_{in} - CO_{out}}{CO_{in}} \times 100$$

C1–C6 products were separated by an alumina-plot column and quantified on the FID detector, from which it was possible to determine the C_{5+} selectivity (S_{C5+}). The CO_2-free S_{C5+} (i.e., S_{C5+} if excluding CO_2 from the C-atom balance) is defined as follows [28,32]:

$$S_{C5+}=100-(S_{C1}+S_{C2}+S_{C3}+S_{C4})_{CO2\ free}$$

Results and Discussion

Synthesis approach

Zr-Al co-precipitated in water-in-oil microemulsion: Several microemulsions were prepared in order to define the composition and temperature of the water/surfactant/oil (W/S/O) system at which the microemulsion was formed and stable. The selected weight ratio in percentages was 7.9/26.4/65.7 **(Table 1)**. The Zr-Al_2O_3 precursor was formed by collision and coalescence of water droplets between microemulsions 1 and 2 (ME1 and ME2). Oxo-hydroxo complexes of zirconium and aluminum were produced when the base came in contact with the metal initiating the nucleation and formation of the first particles inside the water droplets [18,35]. The simultaneous co-precipitation of the precursors inside the water droplets favors in this way a good dispersion of Zr in alumina, and uniform growth of the particles. In addition, the EDX spectra of the material showed Al/Zr/Co atomic ratios **(Table 2)** similar to the added metals. These results show that both Zr and Al precipitated during the synthesis and no loss of metal was detected.

Wetness impregnation: The commercial alumina used as support has a pseudo Y-Al_2O_3 porous structure. This framework allows the deposition of zirconium first and after cobalt oxides inside the pores and on the surface of the alumina. During the calcination step, decomposition of the precursors and reactions between the Zr, Co and Y-Al_2O_3 might occur.

Characterization of the materials

X-Ray diffractograms: The X-ray diffractograms of the carriers and Co-catalysts are illustrated in **Figure 1**. The Zr-Al_2O_3(ME) support presents a low crystalline Y-Al_2O_3 phase. In addition,

Table 2 Representative EDX elemental analysis of the supports and the catalysts.

Material	Al/Zr Atomic ratio	Al/Co Atomic ratio
Zr-Al_2O_3 (IM)	7.9	-
Z-Al_2O_3 (ME)	7.9	-
Co/Zr-Al_2O_3(IM)	8.1	6.8
Co/Zr-Al_2O_3 (ME)	7.9	7.1

no Zr species were detected which might be attributed to the applied synthesis method. One explanation could be that Zr is encapsulated in the alumina matrix and consequently Zr oxide species crystal formation was inhibited [36,37]. In contrast, the Zr-Al_2O_3(IM) material presents characteristic peaks for Υ-Al_2O_3 and a band at 2θ=32° assigned to a metastable ZrO_2 with orthorhombic structure **(Figure 1)**.

After Co deposition, the XRD patterns (**Figure 1** right) showed a highly crystalline Co_3O_4 species were formed in all the catalysts with similar crystallite sizes of approximately 11 nm **(Figure 1 and Table 3)**. Thus, it can be concluded that the presence of Zr does not affect the Co_3O_4 particle size.

N_2 physisorption: The catalyst porosity is presented in **Figure 2**. The isotherms correspond to type IV [38]. The hysteresis loop for Co/Zr-Al_2O_3(ME), corresponds to type H2(b) [38], associated with complex pore networks consisting of pores with ill-defined shapes in the mesopore range. Materials with textural porosity formed by voids between particles can be associate with type H2(b). In addition, this material showed narrow pore size distribution**.** Co**/** Zr-Al_2O_3(IM) and Al_2O_3 supports showed type H3 hysteresis loop [38], correspondent to materials with non-rigid aggregates and wide pore size distribution like amorphous alumina. The carrier isotherms were similar and therefore not included in **Figure 2**.

The surface area for all materials was between 190 and 248 m^2/g **(Table 3)**. Incorporation of Co and/or Zr phases on alumina leads to a decrease in BET surface area and pore volume **(Table 3)**, due to partial pore blockage of the deposited oxides inside the pores [39,40]. The Co_3O_4 particle size was smaller than the Al_2O_3 and Zr-Al_2O_3(IM) pore size, therefore Co_3O_4 deposition is favored inside the pores. On the other hand, Zr-Al_2O_3(ME) had smaller pore diameter sizes than the Co_3O_4 particles **(Table 3),** which leads to the conclusion that some of the Co_3O_4 was deposited on the carrier surface.

Scanning and transmission electron microscopy: The Zr-Al_2O_3(ME) and Co/Zr-Al_2O_3(ME) morphology **(Figure 3)** showed non-agglomerated uniform particle size distribution. However, Co/Al_2O_3, Zr-Al_2O_3(IM) and Co/Zr-Al_2O_3(IM) showed heterogeneous spherical agglomerations of smaller particles of 120, 80 and 80 μm respectively. These agglomerations are attributed to Zr and/or Co deposition. Zr-Al_2O_3(ME) does not agglomerate after cobalt deposition **(Figure 3)**. Based on these findings, it is considered that Zr prevents particle agglomeration, especially when Zr is highly dispersed.

For a better understanding of the species and morphology in the promoted-catalysts, TEM pictures were taken **(Figure 4)**.

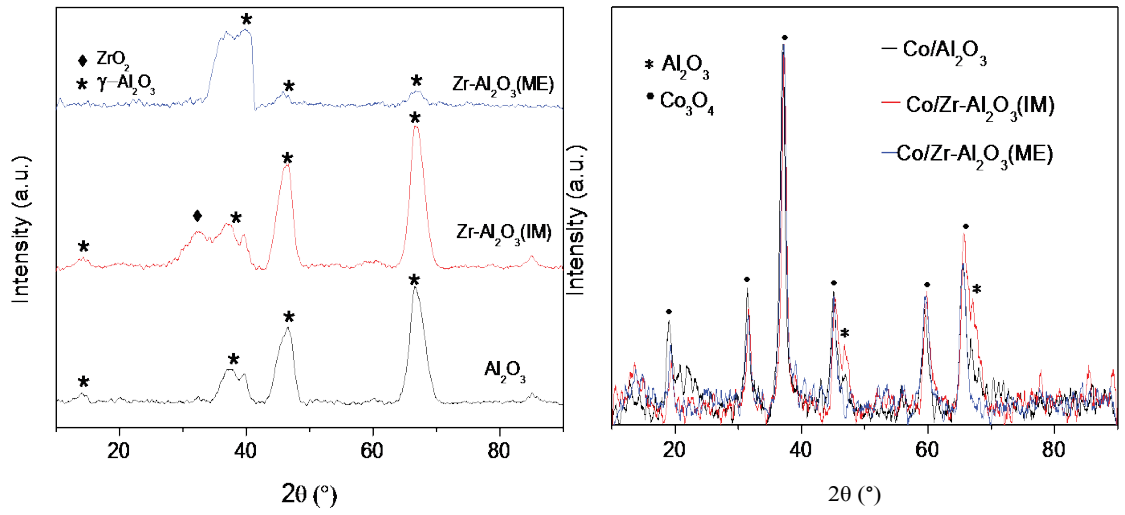

Figure 1 X-ray diffractograms of the carriers (left) calcined at 500°C for 6 h and cobalt-catalysts (right) calcined at 350°C for 10 h.

Table 3 Physicochemical characterization of the supports and catalysts [a] Determined from a single point of adsorption at P/P_0=0.998.[b] Estimated by BJH formalism (adsorption branch). [c] Average crystallite size of Co_3O_4 estimated from Scherrer equation.[d] According with: $d(Co^0)= 0.75 \cdot d(Co_3O_4)$. [e] According to: $d(Co^0)_H = \frac{96}{D} \cdot DOR$.[f] Metal dispersion, after reduction at 350 °C for 16 h in H_2.[i] Degre of reduction (DOR) from TPR of reduced catalysts.

Sample	N_2 Physisorption			XRD		Chemisorption		TPR
	BET Surface area (m^2/g)	Total Pore volume[a] (cm^3/g)	Average Pore diameter (nm)[b]	Particle size Co_3O_4 (nm)[c]	Particle size Co^0 (nm)[d]	Particle size Co^0 (nm)[e]	Metal Dispersion %D[f]	DOR[i]
Al_2O_3	283	1.1	14.7	-	-	-	-	-
Zr-Al_2O_3(IM)	239	0.8	14.0	-	-	-	-	-
Zr-Al_2O_3 (ME)	211	0.3	6.5	-	-	-	-	-
Co/Al_2O_3	248	0.9	14.0	10.5	7.9	26	4.5	30
Co/Zr-Al_2O_3(IM)	227	0.7	12.7	11.3	8.5	27	8.0	47
Co/ZrAl_2O_3 (ME)	191	0.3	5.8	11.3	8.5	41	7.0	11

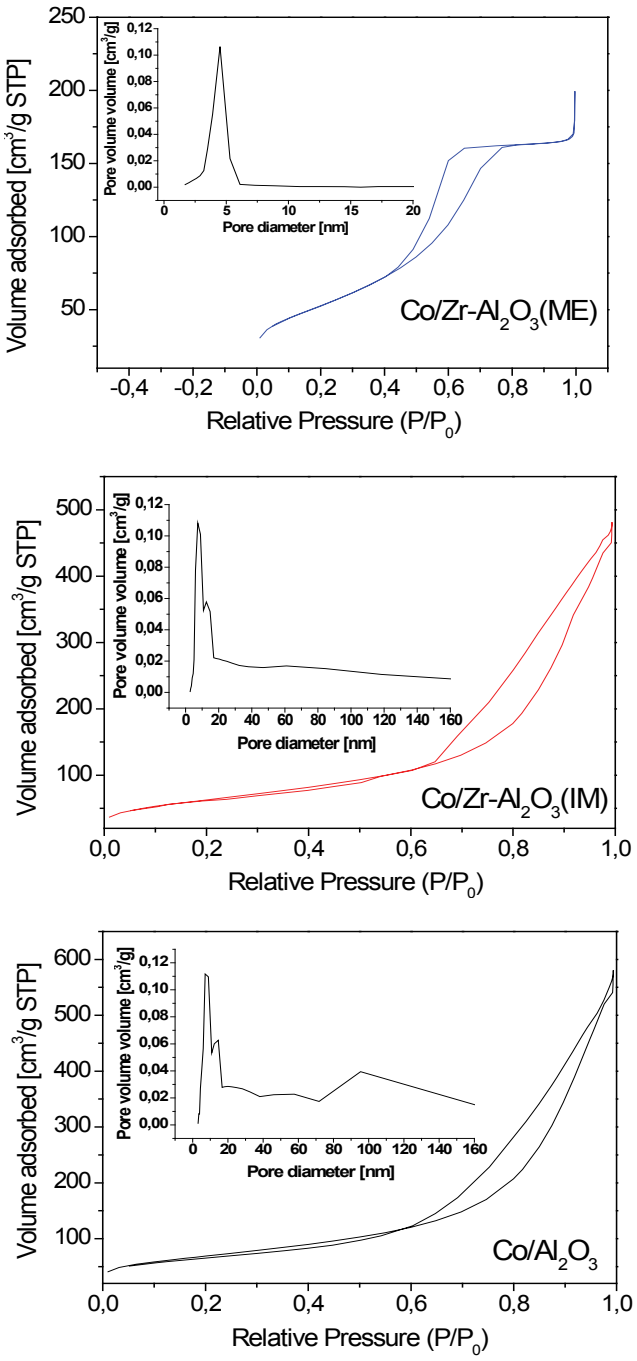

Figure 2 The N_2 adsorption-desorption isotherms and pore size distribution curves for the cobalt catalysts.

Co/Zr-Al_2O_3(ME) shows a homogeneous material formed by agglomerated nanoparticles. Co/Zr-Al_2O_3(ME) shows carrier particle sizes between 4-7 nm and Co_3O_4 cubic crystals **(Figure 4a)**. STEM-EDX mapping results show a homogeneous distribution of Zr on Co/Zr-Al_2O_3(ME) **(Figure 4a)**. This picture demonstrates how the ME technique can be applied for the synthesis of highly disperse oxide promoter on a carrier. The Zr dispersion on alumina in Co/Zr-Al_2O_3(IM) **(Figure 4b)** was lower, forming Zr-rich islands on the Al_2O_3 surface. Furthermore, the cobalt deposition seems to be better in the ME material than in the Zr-impregnated material.

H_2-Temperature programmed reduction: A typical TPR profile for all the catalysts is shown in **Figure 5**. In general, the first two peaks correspond to the reduction of $Co_3O_4 + H_2 \rightarrow 3CoO + H_2O$ [41] and $3CoO + 3H_2 \rightarrow 3Co^0 + 3H_2O$ [42]. The peak around 700°C is attributed to Co_3AlO_6 (Co_3O_4-AlO_2) and/or CoO-Al_2O_3, and the peak at 900°C corresponds to $CoAl_2O_4$ [43-45].

Co_3O_4 in Co/Zr-Al_2O_3(ME) was harder to reduce, as a consequence the reduction temperature was shifted towards higher temperature compared to the other catalysts. The lack of crystallinity in the ME carrier favored the cobalt-aluminate formation and also its reduction temperature.

The TPR for Co/Zr-Al_2O_3(IM) presents similar peaks as for Co/Al_2O_3 with the difference that the reduction temperature was lower by about 50°C. In addition an extra H_2 uptake was seen at 608°C which can correspond to the partial reduction of Zr. The amount of cobalt aluminate species was decreased compared with Co/Al_2O_3, attributed to the presence of Zr. $CoAl_2O_4$ (spinel) was not detected by the XRD technique since its diffractogram peaks overlaps the Co_3O_4 peaks.

Additionally, TPR experiments (**Figure 5** right) were performed after the catalyst activation in order to identify the unreduced cobalt amount and consequently the degree of reduction (DOR) (i.e., from 350 to 930°C in H_2). Co_3O_4 in Co/Zr-Al_2O_3(IM) is completely reduced after catalyst activation with a DOR of 47 %, while the DOR for Co/Al_2O_3 and for Zr-Al_2O_3(ME) is 30 % and 11%, respectively **(Table 3 and Figure 5)**. Thereafter, it can be concluded that the presence of Zr in islands as is the case of Co/Zr-Al_2O_3(IM) decrease the cobalt-alumina interactions, favoring in this way a more metallic formation which is required for a CO hydrogenation reaction.

Interesting to note in all the catalysts (**Figure 5** right) is that the unreduced cobalt species (peaks around 700 and 900°C) shifted the reduction temperature to higher temperatures compared with the first TPR analysis (**Figure 5** left). The explanation given is that during catalysts activation, the remaining unreduced-cobalt in the form of Co° interacts with water (produced by the metal reduction) to form Co-aluminate which is reduced at a higher temperature [15].

Table 3 presents the dispersion of metallic cobalt Co° calculated by H_2 chemisorption (illustrated in experimental part). The results show that Co° dispersion is quite similar in Co/Zr-Al_2O_3(IM) and Co/Zr-Al_2O_3(ME). These results compared with Co/Al_2O_3 are higher, so it is concluded that Zr favors the dispersion of cobalt in alumina support. In addition, the measured Co° particle size by this technique and by TEM is higher than the calculated from the Scherrer equation, from which it can be concluded that during catalyst activation the metallic particles are sintered. This effect is higher in Co/Zr-Al_2O_3(ME) and one of the explanations might be due to the textural porosity and the lack of structural porosity which makes the cobalt-sintering easier.

Catalytic test

Comparing CO conversions for all the catalysts after 25 h of syngas stream (H_2:CO=2.1) **(Table 4)**, the catalyst activity decreases in the following order: Co/Zr-Al_2O_3(IM)>Co/Al_2O_3>Co/Zr-Al_2O_3(ME). The

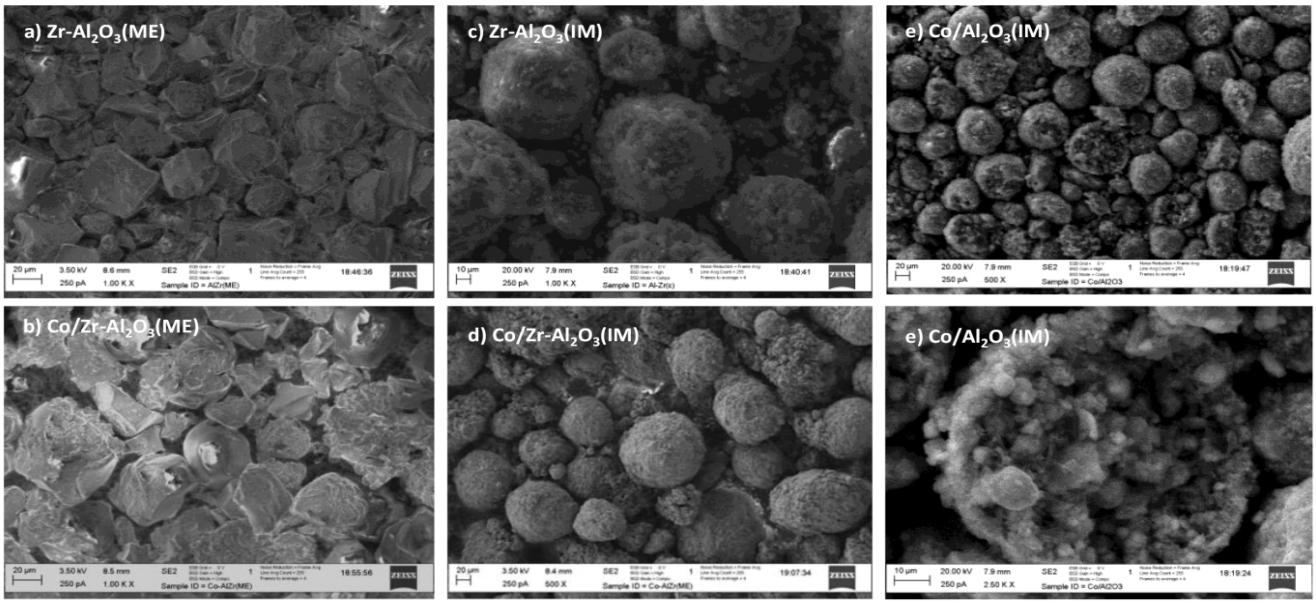

Figure 3 SEM pictures for the carrier and the cobalt catalysts.

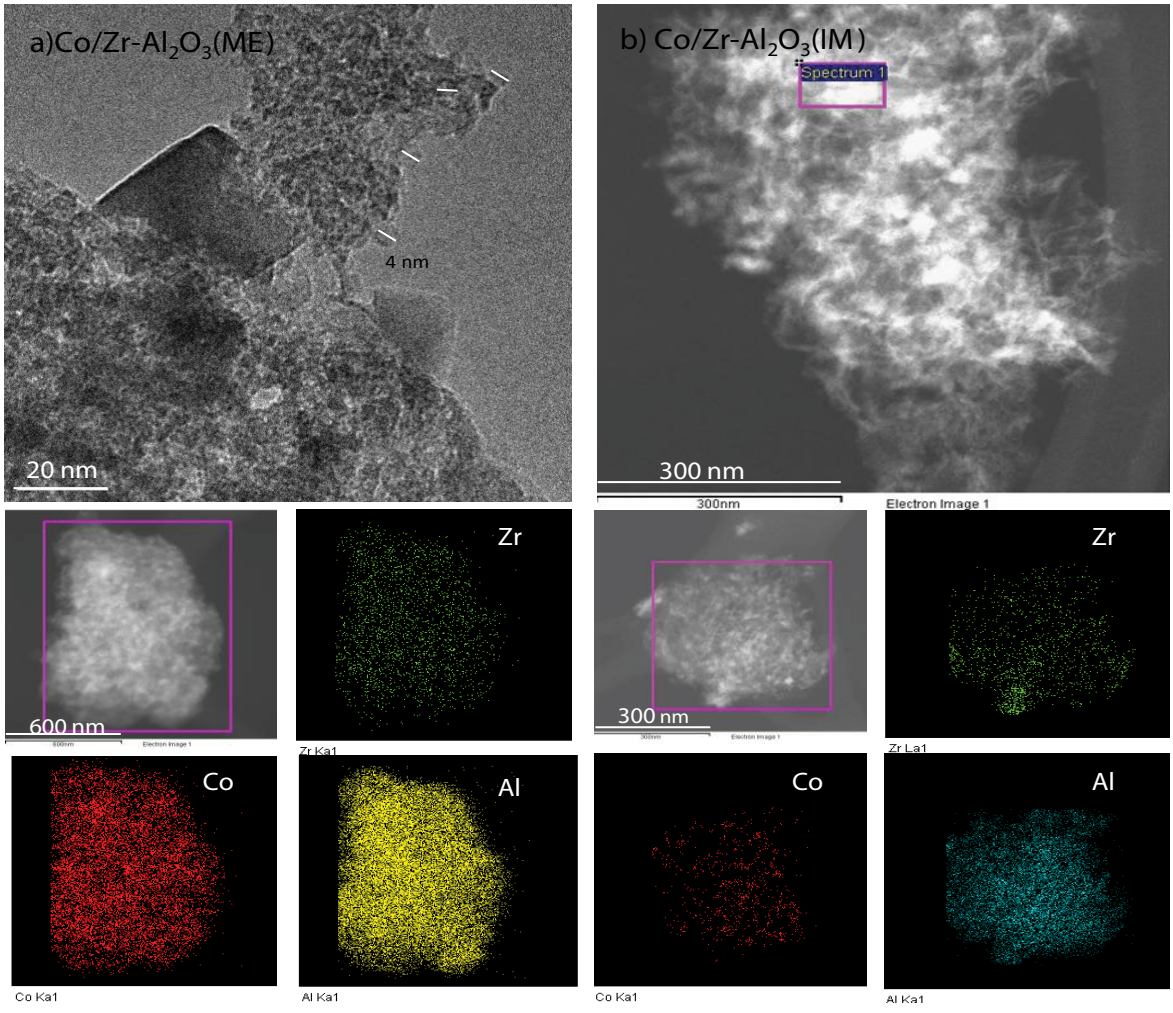

Figure 4 Representative STEM-EDX elemental mapping for a) Co/Zr-Al2O3(ME) and b) Co/Zr-Al2O3(IM).

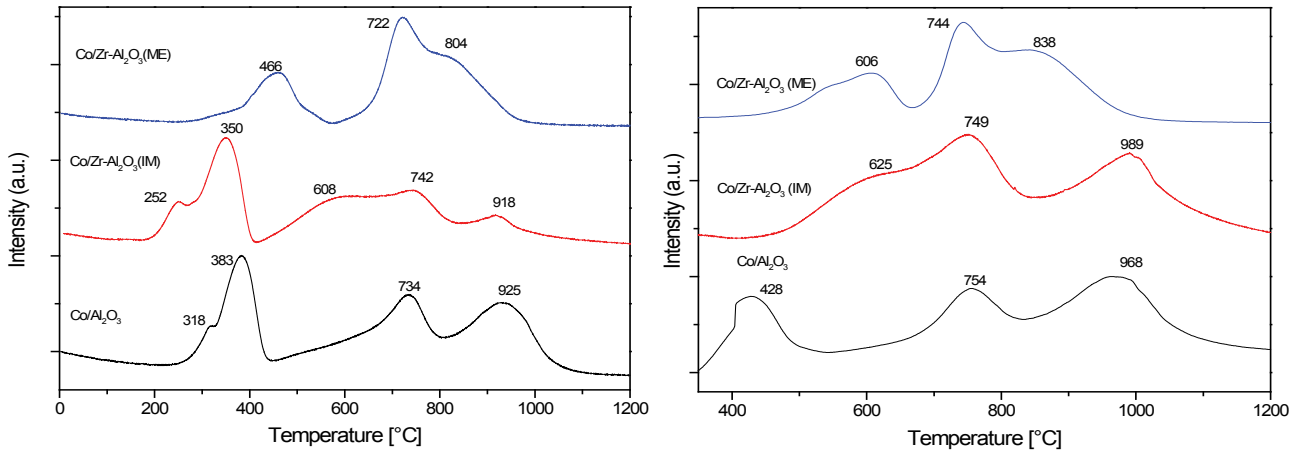

Figure 5 TPR profile for the fresh catalyst (left) and after activation at 350°C for 16 h (right).

Table 4: CO conversion levels and selectivity data for the different catalysts

[a] Selectivities are $CO_{2\text{-free}}$

GHSV ($Ncm^3/(g,h^{-1})$)	Catalysts	X_{CO} (%)	S_{CH4} [a] (%)	S_{C2-C4} [a] (%)	S_{C5+} [a] (%)	S_{CO2} (%)
6000	Co/Al_2O_3	6.5	12.0	12.0	75.0	1.0
1500	Co/Al_2O_3	28.0	8.5	11.0	80.0	0.5
6000	$Co/Zr\text{-}Al_2O_3$ (IM)	12.0	10.0	7.8	81.0	1.2
2350	$Co/Zr\text{-}Al_2O_3$ (IM)	31.0	7.6	6.0	86.0	0.4
6000	$Co/Zr\text{-}Al_2O_3$ (ME)	4.0	20.0	16.0	61.0	3.0
1000	$Co/Zr\text{-}Al_2O_3$ (ME)	27.0	17.0	15.0	67.0	1.0

results are related to: the higher the DOR (degree of reduction of Co) the higher the CO conversion in period one **(Table 3)**.

In all the cases, the selectivity is affected by the CO conversion; the higher the CO conversion, the higher the C_{5+} selectivity (S_{C5+}) and as a consequence the selectivity to CH_4 and C_2-C_4 are decreased. The selectivity to CH_4 and C_2-C_4 were higher for the ME catalyst during both periods; this might be attributed to two facts: low Co^0 formation in the $Co/Zr\text{-}Al_2O_3$ (ME) catalyst and the small pore size of the carrier, around 4 nm, leading to internal mass transfer limitations favoring the faster H_2 diffusion due to its smaller size compared to the CO molecule which diffuses more slowly. This led to higher H_2/CO ratios within the catalyst particles than at the pellet surface.

Conclusion

For the first time, Zr-Al oxides nanoparticles were synthesized by the water-in-oil micro emulsion method. The material presented a high Zr dispersion in alumina and it was highly homogeneous, with uniform particle size, narrow pore size distribution and high surface area. This material was used as cobalt support and compared with similar material prepared by Zr impregnated on commercial alumina. The presence of ZrO_2-islands on alumina favored the dispersion and degree of reduction of cobalt, while the high Zr dispersion in the $Zr\text{-}Al_2O_3$ (ME) material hindered ZrO_2 crystallization. This produced a more amorphous material, leading to a higher degree of $CoAl_2O_4$ formation and therefore increased selectivity to methane and short-chain hydrocarbons C_2-C_4. The catalytic activity and S_{C5+} is favoured by the $Co/Zr\text{-}Al_2O_3$ (IM) catalyst. These results are attributed to the catalyst porosity and higher Co^0 availability on the surface. However, even if the cobalt on $Zr\text{-}Al_2O_3$ nanoparticles (prepared by water-in-oil micro emulsion) is not the best catalyst for CO hydrogenation reaction, when a high C_{5+} selectivity is desired; the material has very good properties to be considered for other applications: such as based material in three-way-catalyst; or as catalyst support for other catalytic reaction like hydrodesulphurization, or to stabilize alumina phases when it is used at high temperatures.

Acknowledgments

Swedish International Development Cooperation Agency (SIDA), Nanoandes network and European project COST Action: CM1101 for financial support. Special thanks to Dr. Emanuela Negro (Deft University of Technology), Edgar Cardenas (Luleå University) and Cesar Leyva Porras (CIMAV, S.C.) for measurements of TEM, SEM and HRTEM/STEM.

References

1 Thomas JM (2009) Handbook of Heterogeneous Catalysis. In: Angewandte Chemie International Edition, Wiley-VCH Verlag: Weinheim 48: 3390-3391.

2 Dry ME (2002) The fischer–tropsch process: 1950–2000. Catal Today 71: 227-241.

3 Suárez PR, Lopez L, Barrientos J, Pardo F, Boutonnet M, et al. (2015) Catalytic conversion of biomass-derived synthesis gas to fuels.

4 Van de Loosdrecht J, Botes FG, Ciobica IM, Ferreira AC, Gibson P, et al. (2013) Fischer–Tropsch Synthesis: Catalysts and Chemistry Elsevier: Amsterdam pp: 525-557.

5 Grenoble DC, Estadt MM, Ollis DF (1981) The chemistry and catalysis of the water gas shift reaction: 1. The kinetics over supported metal catalysts. J Catal 67: 90-102.

6 Tsakoumis NE, Rønning M, Borg Ø, Rytter E, Holmen A (2010) Deactivation of cobalt based Fischer–Tropsch catalysts: A review. Catal Today 154: 162-182.

7 Borg Ø, Eri S, Blekkan EA, Storsæter S, Wigum H, et al. (2007) Fischer–Tropsch synthesis over γ-alumina-supported cobalt catalysts: Effect of support variables. J Catal 248: 89-100.

8 Moradi GR, Basir MM, Taeb A, Kiennemann A (2003) Promotion of Co/SiO_2 Fischer–Tropsch catalysts with zirconium. Catal Commun 4: 27-32.

9 Miyazawa T, Hanaoka T, Shimura K, Hirata S (2014) Fischer–Tropsch synthesis over a Co/SiO_2 catalyst modified with Mn- and Zr under practical conditions. Catal Commun 57: 36-39.

10 Miyazawa T, Hanaoka T, Shimura K, Hirata S (2013) Mn and Zr modified Co/SiO_2 catalysts development in slurry-phase Fischer–Tropsch synthesis. Applied Catalysis A: General 467: 47-54.

11 Liu Y, Chen J, Fang K, Wang Y, Sun Y (2007) A large pore-size mesoporous zirconia supported cobalt catalyst with good performance in Fischer–Tropsch synthesis. Catal Commun 8: 945-949.

12 Li Z, Wu J, Yu J, Han D, Wu L, et al. (2016) Effect of incorporation manner of Zr on the Co/SBA-15 catalyst for the Fischer–Tropsch synthesis. J Mol Catal A Chem 424: 384-392.

13 Shimura K, Miyazawa T, Hanaoka T, Hirata S (2015) Fischer–Tropsch synthesis over alumina supported cobalt catalyst: Effect of promoter addition. Applied Catalysis A: General 494: 1-11.

14 Enache DI, Roy-Auberger M, Revel R (2014) Differences in the characteristics and catalytic properties of cobalt-based Fischer–Tropsch catalysts supported on zirconia and alumina. Applied Catalysis A: General 268: 51-60.

15 Rohr F, Lindvåg OA, Holmen A, Blekkan EA (2000) Fischer–Tropsch synthesis over cobalt catalysts supported on zirconia-modified alumina. Catal Today 58: 247-254.

16 Jongsomjit B, Panpranot J, Goodwin JG (2003) Effect of zirconia-modified alumina on the properties of $Co/\gamma\text{-}Al_2O_3$ catalysts. J Catal 215: 66-77.

17 Jacobs G, Das TK, Zhang Y, Li J, Racoillet G, et al. (2002) Fischer–Tropsch synthesis: support, loading, and promoter effects on the reducibility of cobalt catalysts. Applied Catalysis A: General 233: 263-281.

18 Boutonnet M, Marinas A, Montes V, Suárez-Paris R, Sánchez-Domınguez M (2016) Nanocatalysts: Synthesis in Nanostructured Liquid Media and Their Application in Energy and Production of Chemicals, in Nanocolloids, Elsevier: Amsterdam pp: 211-246.

19 Kombaiah K, Vijaya JJ, Kennedy LJ, Bououdina M, Al-Lohedan HA, et al. (2017) Studies on Opuntia dilenii haw mediated multifunctional $ZnFe_2O_4$ nanoparticles: Optical, magnetic and catalytic applications. Mater Chem Phys 194: 153-164.

20 Singh AK (2016) Structure, Synthesis, and Application of Nanoparticles, in Engineered Nanoparticles, Academic Press: Boston pp: 19-76.

21 Eriksson S, Nylén U, Rojas S, Boutonnet M (2004) Preparation of catalysts from microemulsions and their applications in heterogeneous catalysis. Appl Catal A 265: 207-219.

22 Pardo-Tarifa F, Cabrera S, Sanchez-Dominguez M, Boutonnet M (2017) Ce-promoted Co/Al 2 O 3 catalysts for Fischer-Tropsch synthesis. Int J Hydrogen Energy 42: 9754-9765.

23 Boutonnet M, Sanchez-Dominguez M (2017) Microemulsion droplets to catalytically active nanoparticles. How the application of colloidal tools in catalysis aims to well design and efficient catalysts. Catal Today 285: 89-103.

24 Misono M (2013) Chemistry and Catalysis of Mixed Oxides. Stud Surf Sci Catal 25-65.

25 Sprague MJ (1985) Characterization of heterogeneous catalysts. Chemie Ingenieur Technik 57: 430-430.

26 Lemaitre JL, Delannay PGF (1984) Characterization of Heterogeneous Catalysts, Denker, New York. 299-365.

27 Schanke D, Vada S, Blekkan EA, Hilmen AM, Hoff A, et al. (1995) Study of Pt-promoted cobalt CO hydrogenation catalysts. J Catal 156: 85-95.

28 Lögdberg S, Lualdi M, Järås S, Walmsley JC, Blekkan EA, et al. (2010) On the selectivity of cobalt-based Fischer–Tropsch catalysts: evidence for a common precursor for methane and long-chain hydrocarbons. J Catal 274: 84-98.

29 Reuel RC, Bartholomew CH (1984) The stoichiometries of H2 and CO adsorptions on cobalt: Effects of support and preparation. J Catal 85: 63-77.

30 Jones RD, Bartholomew CH (1988) Improved flow technique for measurement of hydrogen chemisorption on metal catalysts. Appl Catal 39: 77-88.

31 Bhatia S, Beltramini J, Do DD (1990) Temperature programmed analysis and its applications in catalytic systems. Catal Today 7: 309-438.

32 Lualdi M, Lögdberg S, Regali F, Boutonnet M, Järås S (2011) Investigation of mixtures of a Co-based catalyst and a Cu-based catalyst for the Fischer–Tropsch synthesis with bio-syngas: the importance of indigenous water. Top Catal 54: 977-985.

33 Storsæter S, Borg Ø, Blekkan EA, Holmen A (2005) Study of the effect of water on Fischer–Tropsch synthesis over supported cobalt catalysts. J Catal 231: 405-419.

34 Lualdi M (2012) Fischer-Tropsch Synthesis over Cobalt-based Catalysts for BTL Applications.

35 Boutonnet M, Lögdberg S, Svensson EE (2008) Recent developments in the application of nanoparticles prepared from w/o microemulsions in heterogeneous catalysis. Curr Opin Colloid Interface Sci 13: 270-286.

36 Chandradass J, Kim KH (2009) Effect of acidity on the citrate-nitrate

combustion synthesis of alumina-zirconia composite powder. Met Mater Int 15: 1039-1043.

37 Baudín C (2014) Processing of Alumina and Corresponding Composites. Comprehensive Hard Materials 31: 72.

38 Thommes M, Kaneko K, Neimark AV, Olivier JP, Rodriguez-Reinoso F, et al. (2015) Physisorption of gases, with special reference to the evaluation of surface area and pore size distribution .Pure Appl Chem 87: 1051-1069.

39 Martínez A, Prieto G, Rollán J (2009) Nanofibrous γ-Al_2O_3 as support for Co-based Fischer–Tropsch catalysts: pondering the relevance of diffusional and dispersion effects on catalytic performance. J Catal 263: 292-305.

40 Liu C, Li J, Zhang Y, Chen S, Zhu J, et al. (2012) Fischer–Tropsch synthesis over cobalt catalysts supported on nanostructured alumina with various morphologies. J Mol Catal A: Chem 363: 335-342.

41 Castner DG, Watson PR, Chan IY (1990) X-ray absorption spectroscopy, X-ray photoelectron spectroscopy, and analytical electron microscopy studies of cobalt catalysts. 2. Hydrogen reduction properties. J Phys Chem 94: 819-828.

42 Øyvind B, Magnus R, SØlvi S, Anders H (2007) Identification of cobalt species during temperature programmed reduction of Fischer-Tropsch catalysts. Studies in Surface Science and Catalysis 163: 255-272.

43 Topsøe NY, Topsøe H (1982) Adsorption studies on hydrodesulfurization catalysts: I. Infrared and volumetric study of NO adsorption on alumina-supported Co, Mo, and Co-Mo catalysts in their calcined state. J Catal 75: 354-374.

44 Simionato M, Assaf EM (2003) Preparation and characterization of alumina-supported Co and Ag/Co catalysts. Mater Res 6: 535-539.

45 Van de Loosdrecht J, Van der Haar M, Van der Kraan AM, Van Dillen AJ, Geus JW (1997) Preparation and properties of supported cobalt catalysts for Fischer-Tropsch synthesis. Appl Catal A 150: 365-376.